Research Article

The Effect of the Hump Position of the Wings on Aerodynamic Parameters

Authors: Ramazan SELVER iD , Yusuf Can AKAR iD

To link to this artice: https://dergipark.org.tr/tr/pub/ijeir/archive

The Effect of the Hump Position of the Wings on Aerodynamic Parameters

Ramazan SELVER [1] , Yusuf Can AKAR[2*]

[1]Süleyman Demirel University, Faculty of Engineering, Department of Mechanical Engineering, 32200, Isparta, Türkiye
[2]Süleyman Demirel University, Institute of Science and Technology, Department of Mechanical Engineering, 32200, Isparta, Türkiye

*Corresponding Author: yusufcan2306@gmail.com
(**Received:** 31.05.2023; **Accepted:** 24.07.2023)

Abstract: In this article, the aerodynamic performances of 3D wings coded NACA 6415 and NACA 6615 are investigated at different angles of attack and speeds. Analyzes were performed at 200 km/h and 700 km/h speeds, between 0 and 36 degrees angle of attack. The obtained results showed the changes in lift, drag and moment coefficients depending on the angle of attack and speed of the wings. In addition, it was determined that the highest lift/drag ratios for both wing types were obtained at 0 degrees angle of attack. These results can be used as a reference source for the aerospace industry.

1. INTRODUCTION

One of the pioneers of aerodynamic studies that gained momentum after World War II, NACA (now known as NASA) started producing wing profiles for aircraft. Wings are profile structures used to generate lift force. The naming of the sections of a airfoil is shown in Figure 1.
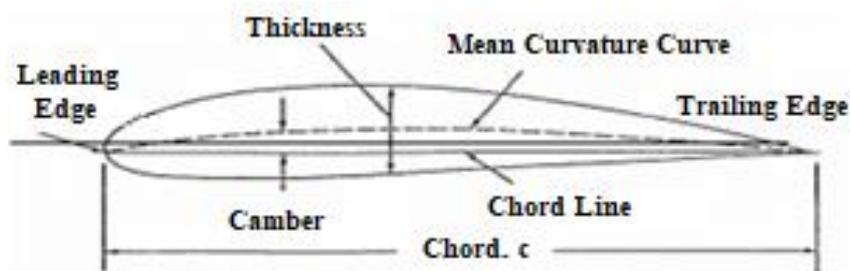

Figure 1. For captions, please use the figure description style [1]

When studying the wing structure, the part of the wing that first comes into contact with the air is called the leading edge, while the part where the air separates from the wing is called the trailing edge. The line that connects these points is called the chord line. The curve that passes through the center of the upper and lower surfaces and connects the leading and trailing edges is called the camber curve [2].

Wings are numbered according to the ratios of these lines. If we examine the NACA 6415 wing, the first digit 6 indicates that the wing has a maximum camber ratio of 6%. The second digit 4 indicates that the wing's maximum camber is located 40% of the distance from the leading edge.

From the last two digits being 15, we understand that the wing's maximum thickness is 15% of the chord length [3].

As with many other fields, the method of dimensional analysis has been utilized in aerodynamics as well. In the case of wings, the dimensionless forms of forces are more meaningful. The formulas for the dimensionless forms of lift force, pitching moment, and drag force are shown in Table 1.

Table 1. The fundamental dimensionless quantities in aerodynamics[4]

Physical Quantities	Unit	Dimensionless Form
Drag Force (D)	Newton	$C_D = \dfrac{D}{\frac{1}{2}\rho V_\infty^2 S}$
Pitching Moment (M)	Newton meter	$C_M = \dfrac{M}{\frac{1}{2}\rho V_\infty^2 S c}$
Lift Force (L)	Newton	$C_L = \dfrac{L}{\frac{1}{2}\rho V_\infty^2 S}$

Table 1 shows the dimensionless forms of the lift coefficient C_L, drag coefficient C_D, and moment coefficient C_M. Here, ρ represents the density of air, V_∞ denotes the free stream velocity, S represents the wing reference area, and c represents the wing chord length.

The lift force is the upward force on the aircraft's wing caused by the pressure difference between the upper and lower surfaces of the wing. The drag force is also known as the required motor force. The pitching moment is the moment that moves the leading edge of the wing clockwise or counterclockwise along the wing's chord line. A clockwise moment is considered positive.

The airflow over the top surface of the aircraft wing flows faster due to the wing's shape and angle. This faster flow creates low-pressure areas on the wing's upper surface according to the Bernoulli equation. These low-pressure areas are lower than the air pressure on the wing's lower surface, causing the wing to generate an upward lift force. The generated lift force increases as the angle of attack of the wing increases. However, if the angle of attack of the wing is too high, the airflow over the wing's surface can separate, causing the lift force to suddenly decrease or completely disappear. The separation of the airflow over the wing's upper surface indicates that the wing has "stalled". In this case, the lift force generated by the wing decreases or disappears.

Another factor that affects the stall condition is the speed of the airflow. Even if the wing has not reached high angles of attack, a decrease in airspeed can cause the wing to enter a stall condition. To understand how the stall condition appears on the wing, the image of a wing in stall condition used in this study is provided in Figure 2.
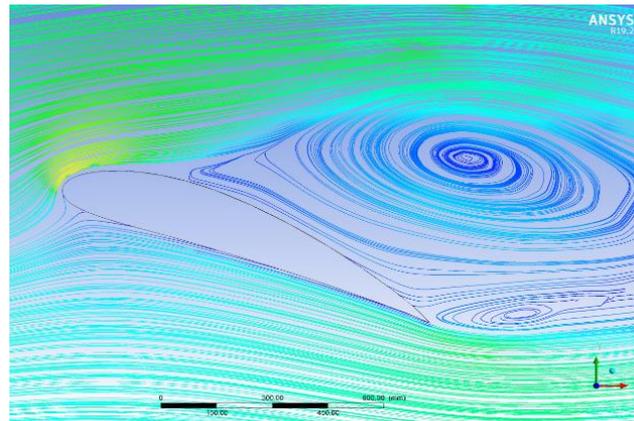
Figure 2. Streamlines of a wing in a stall condition.

2. MATERIAL and METHODS

In this study, ANSYS 19.2 program's "Fluent" package was used for numerical solutions of flow analysis and "Static Structural" package was used for static analysis. The coordinates of two wings analyzed, NACA 6415 and NACA 6615, were obtained from the internet [5].

Using these wing coordinate values, geometry was created in the ANSYS program, with a wing span of 1 meter. Two "I" beams were placed on the wing profile to divide the wing into three sections along the X-axis of the wing. The placed 'I' profile beams were positioned to enhance the structural strength of the wing. The beams were extended to 4 meters in length and intermediate profiles of 10 mm were placed on them along the wing at intervals of 10 mm. These intermediate profiles were densely placed on the side of the wing connected to the aircraft body and gradually became sparse towards the other side, creating 7 sections on the wing. Finally, a thickness of 10 mm was given for the outer skin of the wing. The final form of the wing is shown in Figure 3.
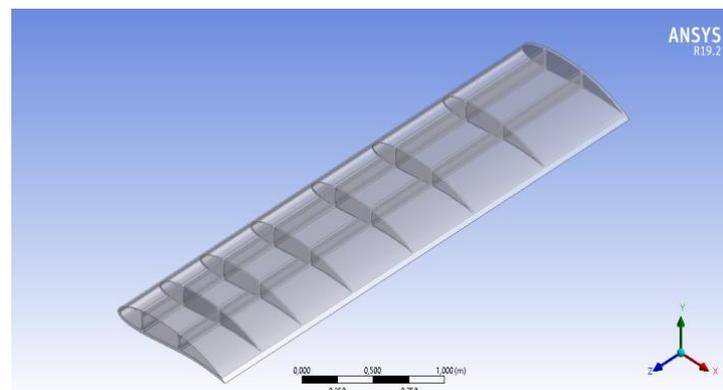

Figure 3. NACA 6615 wing profile

The wing was fixed with the condition of taking the aircraft connection part as the origin, and a control volume was drawn around the wing to represent the airflow. This control volume is shown in Figure 4.
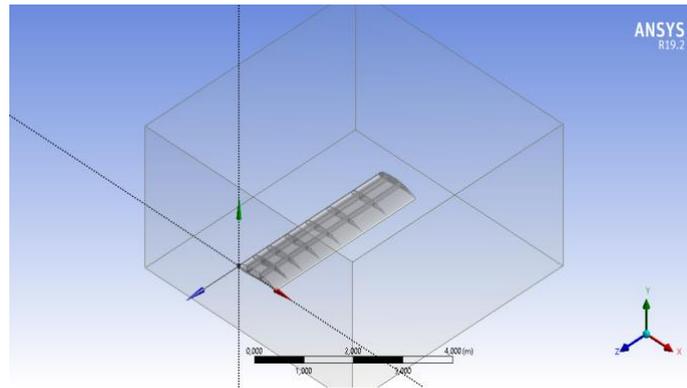
Figure 4. Control volume of airflow

The generated geometry was transferred to the Fluid Flow section. Meshing was applied to the entire volume, with denser meshing near the wing edges. The meshing image is shown in Figure 5.
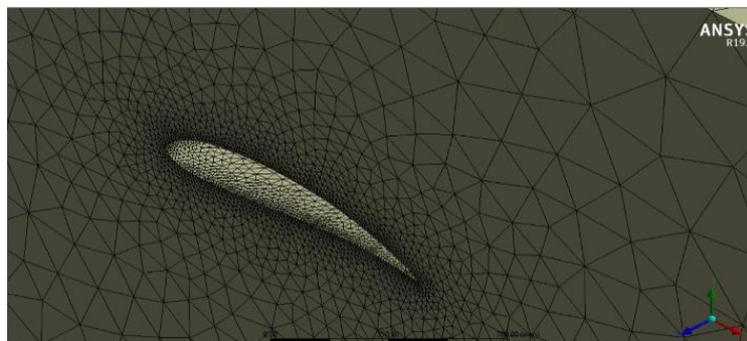

Figure 5. Mesh view of the control volume

After the meshing was completed, the final settings were adjusted from the "Setup" section. The air flow velocity was first set to 200 km/h, then 700 km/h. Since the pressure at the outlet of the air is atmospheric pressure, it was entered as zero (0) Pa. The standard k-epsilon turbulence model was selected as the flow type, and the analysis was started with 2000 iterations.

After the flow analysis was completed, the "static structural" section was used for static analysis. In this section, meshing was performed on the wing itself instead of the air, and the mesh view of the wing is shown in Figure 6.
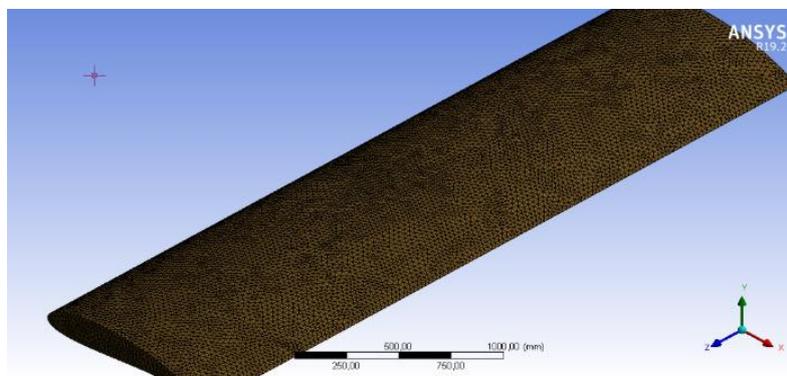

Figure 6. Mesh view of the wing

After the meshing process, two boundary conditions were applied. The first one is the "fixed support" used to fix the wing, and the second one is the "fluid-solid interface" required to apply forces onto the wing. For the fixed support, the part where the wing will be connected to the aircraft was selected, while for the fluid-solid interface, the outer surface of the wing was selected. Afterwards, the desired force and moment reactions to be seen after the analysis were selected from the "results" section.

In the selection of the wing material, the usage ratios in aviation were researched, and accordingly, the material was chosen. Mechanical properties and costs were also taken into consideration, and Aluminum 7075-T6 (Al 7075-T6) was selected as the wing material. The mechanical properties of the material are given in Table 2.

Table 2. The mechanical properties of Al 7075-T6 [6]

Material	Density (g/cm³)	Rupture Stress (MPa)	Shear Stress (MPa)	Yield Stress (MPa)
Al 7075-T6	2.81	572	331	503

Analyses have been conducted for this wing at 0° to 36° angles of attack at 200 km/h and 700 km/h speeds. Then, for comparison with a NACA 6415 wing made entirely of the same dimensions and material, it was analyzed under the same conditions and values. The profiles of the two wings used are given in Figure 7.
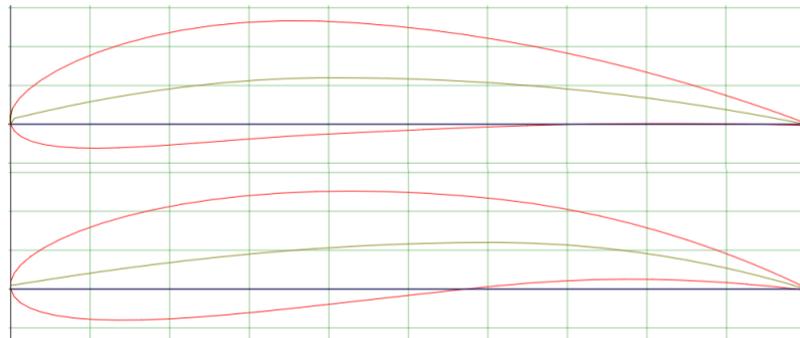

Figure 7. From top to bottom, NACA 6415 and NACA 6615 wing profiles

3. RESULTS and DISCUSSION

The results obtained from the analyses have been presented in the form of graphs. Figure 8 shows the variations of lift coefficients with respect to angle of attack.
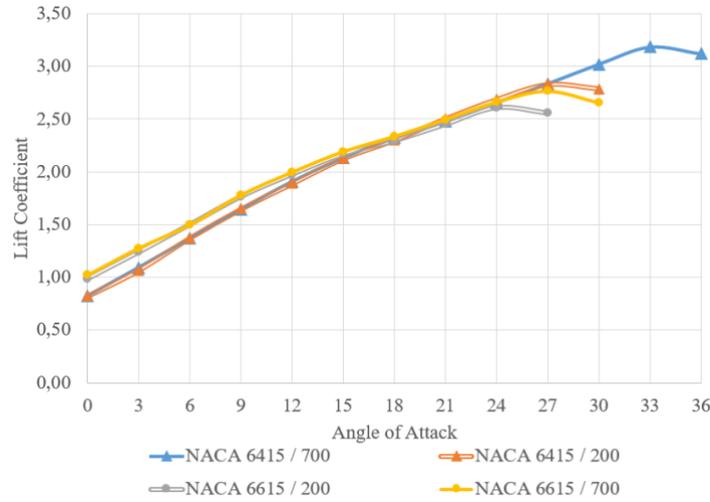
Figure 8. Lift coefficient graph

When examining Figure 8; at 0 degree angle of attack and 200 km/h speed, the lift coefficient of NACA 6415 is 0.823, while NACA 6615 has a lift coefficient of 0.986. At 700 km/h speed and 0 degree angle of attack, the lift coefficient of NACA 6415 is 0.824, while NACA 6615 has a lift coefficient of 1.01.

The NACA 6415 wing reaches its maximum lift coefficient at a 27 degree angle of attack and 200 km/h speed, and at a 33 degree angle of attack and 700 km/h speed. The NACA 6615 wing reaches its maximum lift coefficient at a 24 degree angle of attack and 200 km/h speed, and at a 27 degree angle of attack and 700 km/h speed.

When examining these values, it is seen that the angle at which the wings reach maximum lift coefficient changes according to speed. However, it is observed that the speed of the air does not affect the lift coefficient before reaching the maximum lift.
It is known that the wings enter the stall condition after the maximum lift point, so no further analysis was carried out beyond those angles. Figure 9 shows the variation of the drag coefficients of the wings with respect to the angle of attack.
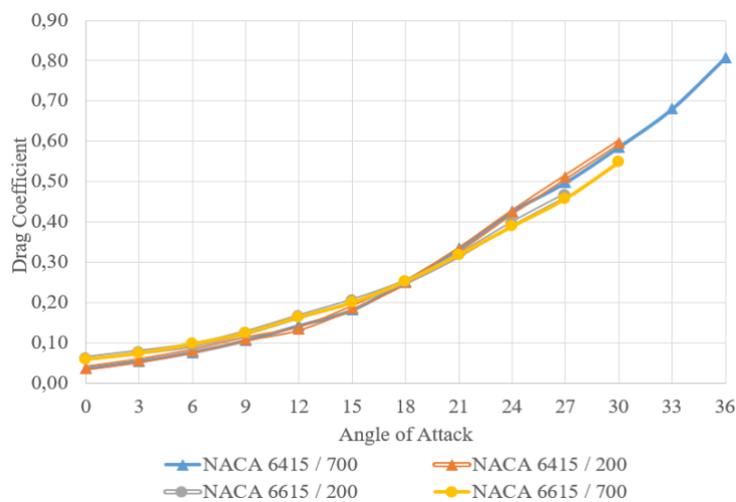

Figure 9. Drag coefficient graph

When Figure 9 is examined, it can be seen that the lift coefficients are independent of speed. In the range of 0-18 degrees angle of attack, NACA 6615 produced more drag coefficient, while NACA 6415 produced more drag coefficient at angles greater than 15 degrees.

In another study of ours, we had observed that the maximum value of the lift coefficient increases in relation to the airflow velocity [7].

Figure 10 shows the variation of the C_L/C_D values of the wings with respect to the angle of attack.
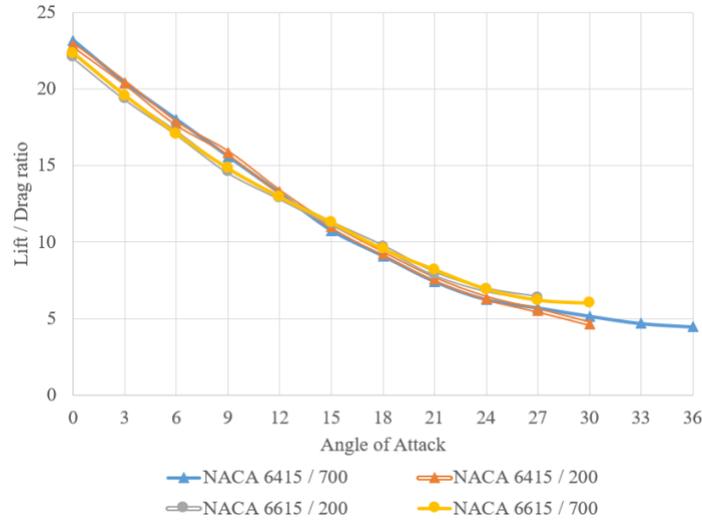

Figure 10. Wing efficiency graph

Figure 10 shows the wing efficiency graph in terms of the lift-to-drag ratio (C_L/C_D) versus angle of attack. This expression represents the amount of lift generated per unit of drag produced by the wing, known as wing efficiency. Upon examining Figure 10, it can be concluded that both wings operate at maximum efficiency at a 0 degree angle of attack. As the angle of attack increases, the efficiency values of the wings decrease. While the NACA 6615 wing initially operates less efficiently than the NACA 6415 wing, it becomes more efficient than the latter at approximately 13 degrees of angle of attack. The rate at which the efficiency decreases with increasing angle of attack is greater in the case of the NACA 6415 wing.

Figure 11 shows the variation of moment coefficients obtained from the pitching moment of the wings with respect to angle of attack.
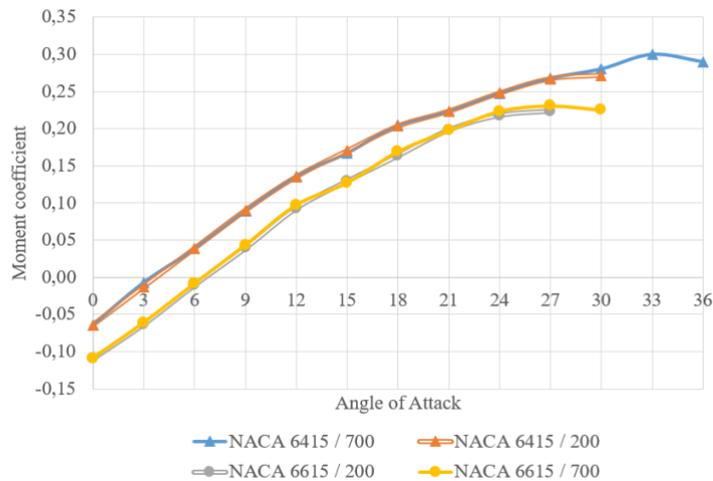

Figure 11. Moment coefficient graph

Figure 11 shows the variations of the pitching moment coefficients of the wings with respect to the angle of attack obtained from the pitching moment balance. When examining Figure 11, it is seen that the wings reach their maximum pitching moment coefficients at the angle of attack where their maximum lift coefficients occur.

NACA 6415 wing still generates a negative pitching moment at 3 degrees angle of attack, while NACA 6615 wing generates a negative pitching moment at 6 degrees angle of attack. It is observed that the moment coefficient value of NACA 6415 wing is greater than NACA 6615 wing at both speed values.

Figure 12 presents the variations of the deflection angles of the wings with respect to the angle of attack.
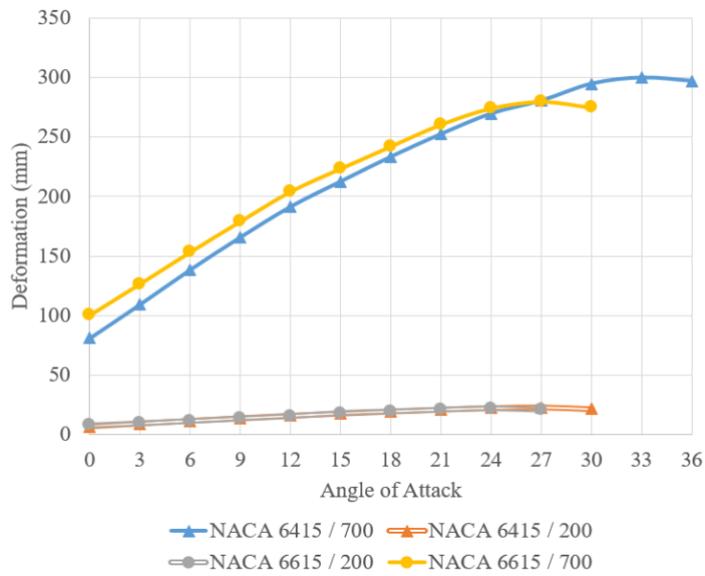

Figure 12. Deformation graph

When Figure 12 is examined, it is observed that the maximum deflection value is reached at the angle of attack where the maximum lift coefficient is obtained. Unlike the previous graphs, the effect of the velocity factor is seen in the deflection values. At high speeds, much larger deflection values are observed due to the larger dynamic force created by the increased speed. Although it is not significant at low speeds, it has been observed that the NACA 6615 wing reaches higher deflection values than the NACA 6415 wing. However, when looking at the maximum deflection value, it is seen that the NACA 6415 wing has reached a higher deflection value.

Figure 13 shows the changes in shear stresses with respect to the angle of attack.
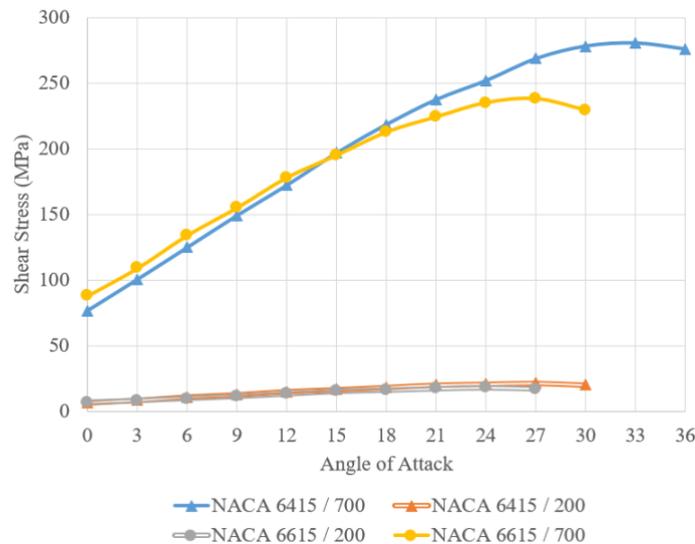
Figure 13. Shear Stress graph

Figure 13 shows the graph of shear stresses. Upon examination of Figure 13, it can be seen that the shear stresses exhibit a similarity to the deformation value graph. Although the NACA 6615 wing is initially subjected to higher stress at a speed of 700 km/h, the NACA 6415 wing experiences more shear stress after a 15-degree angle of attack. It has been observed that the rate of increase in shear stress of NACA 6415 with respect to angle of attack is higher than that of NACA 6615.

6. CONCLUSION and SUGGESTIONS

In this study, two different wing profiles were modeled using Ansys Fluent software, and the aerodynamic parameters of the wings at different speeds were numerically analyzed. Airflow speeds of 200 km/h and 700 km/h were applied to both wings, and the wings were analyzed at certain angles ranging from 0° to 36°.

When the lift coefficients of the wings at 0° angle of attack were examined, we see that NACA 6615 has a higher lift coefficient. As the angle of attack increases, the difference between them decreases and after approximately 18 degrees, this difference disappears. An increase in the lift coefficient means more lift force. In this regard, NACA 6615 has an advantage in terms of lift coefficient.

When looking at the drag coefficients, it is seen that NACA 6615 has a higher drag coefficient between 0-18 angles of attack. However, after this angle, since the increase rate of drag coefficient in NACA 6615 is lower than NACA 6415, NACA 6415 produces more drag coefficient. A high drag coefficient means the aircraft consumes more energy, which is an undesirable situation. In this case, it is seen that NACA 6615 consumes more energy than NACA 6415 after the 0-18 degree range.

To better compare the lift and drag coefficients, the efficiency expressions of the wings were examined. When looking at the CL/CD ratios, it is seen that NACA 6415 works more efficiently in the range of 0° to 12° angle of attack, while NACA 6615 works more efficiently after 12 degrees. It is observed that as the angle of attack increases, the efficiency of the wings decreases. When the moment coefficients were examined, it was observed that taking the maximum camber from 40% to 60% had a negative effect. The NACA 6615 wing produced a lower moment coefficient than the NACA 6415 wing.

Looking at the lift, drag, moment coefficients and efficiency expressions, we see that approximately the same results are obtained at both 200 km/h and 700 km/h speeds. Based on these graphs, we can say that the coefficients produced by the forces generated due to the aerodynamic shape of the wing are independent of the airflow rate. The increase in speed only changed the maximum lift angle, which is due to the increase in the stall angle.

When we look at the deflection and shear stresses of the wings, we see that taking the maximum camber to 60% caused the wing to lose strength at low angles.

In conclusion, the differences between the NACA 6415 and NACA 6615 wings require a selection based on flight conditions and performance requirements. In aircraft design, wing profile shapes should be carefully selected to direct airflow in the most suitable way and balance lift force and resistance.

7. ACKNOWLEDGEMENTS

REFERENCES

[1]   Genç M. S., Özışık G., N. Kahraman, "Investigation of the Aerodynamic Performance of NACA 0012 Wing Profile with Plain Flaps" J. of Thermal Science and Technology, s1-8, 2008.

[2]   Gökdemir M., ÜRGÜN S., "Aerodynamic Analysis of Wing Profiles with Similar Camber", Journal of Aviation, s25-35, 2020.

[3]   Güçlü M. C., Aerodynamic Performance Analysis and Control of Flow Over Airplane Wings: A Master's Thesis in the Institute of Science and Technology at TOBB University of Economics and Technology, Ankara, Türkiye, 2019.

[4]   Akar Y.C., Selver R., Başekin M., "Effect of Hump Ratio of The Wings on Aerodynamic Parameters" 4th International 5 Ocak congress on Applied Sciences Proceeding Book, 5-6 Jan 2023, s.66-74, https://www.inbak.org/_files/ugd/614b1f_b24fcbb45f544624884760221f300690.pdf

[5]   AirfoilTools, Coordinates of NACA 4415, http://airfoiltools.com/airfoil/details?airfoil=naca4415-il,

[6]   Davis J.R. ASM International "Metals Handbook Properties and Selection: Nonferrous Alloys and Special-Purpose Materials Vol.2", 10th Ed. 1990

[7]   Akar Y.C. and Selver R., "The Effect of High-Speed Aif Flows on Different Airfoils", Dicle University Journal of the Institute of Natural and Applied Science c.12, Vol.1, s.65-94, Jun 2023, doi:10.55007/dufed.1129899